Int J Adv Manuf Technol (2016) 83:611–621
DOI 10.1007/s00170-015-7581-5

ORIGINAL ARTICLE

Study on the effects of friction stir welding process parameters on the microstructure and mechanical properties of 5086-H34 aluminum welded joints

H. Mohammadzadeh Jamalian[1] · **M. Farahani**[1] · **M. K. Besharati Givi**[1] · **M. Aghaei Vafaei**[1]

Received: 29 April 2015 / Accepted: 12 July 2015 / Published online: 30 July 2015

Abstract In this study, the effects of tool rotational and traverse speeds on the mechanical properties and the microstructure of the friction stir welded joints from Al 5086-H34 were studied. Insufficient heat generation and inadequate metal transportation at very low rotational speed and high turbulence in the plasticized metal at very high rotational speed emerged tunnel and worm hole defects into the weldment. It was discovered that as rotational and traverse speed increased, the average grain size of the weldment decreased due to more dynamic recrystallization and amplified stirring effect. An increase in the rotational speed increased the ultimate tensile strength and microhardness of the specimens. At the best welding condition, by employing the rotational and traverse speeds of 1250 rpm and 80 mm/min, respectively, 51 % enhancement in the elongation and 8 % increase in the microhardness of the welded samples were obtained. Moreover, the ultimate tensile strength of this welded joint reached to 85 % of the base metal.

Keywords Friction stir welding · Rotation speed · Traverse speed · SEM · 5086-H34 aluminum alloy

1 Introduction

Aluminum is mainly known for its low density and high corrosion resistance. The welding of Al and its alloys has always represented a big challenge for designers and technologists [1]. The conventional joining processes concerning these alloys include gas metal arc welding (GMAW), gas tungsten arc welding (GTAW), plasma arc welding (PAW), and electron beam welding (EBW) [2]. The strength of the joints fabricated through the conventional fusion welding methods can only reach up to 50–70 % of the parent metal. Low strength of these welded joints can be explained by segregation, low melting temperature, porosities, and loss of alloying elements during the conventional fusion welding processes. Large amount of residual stresses induced by fusion welding process also decreases the strength of the welded joints [3–5]. Welding-distortion or warping of weldments during fusion welding is another problem of conventional welding which is a natural outcome of the high amount of welding heat input and consequently large internal stresses produced during the conventional welding [6]. Due to these problems, the weldability of the aluminum alloys is classified as "difficult to weld" metals [7].

On the other side, it was reported that the ultimate strength of the welded joints produced by friction stir welding (FSW) technique reached 80–100 % of the parent metal [8]. FSW is a solid-state joining process proposed at the TWI organizations in 1991 in which a rotating tool is plunged into the workpieces and traverses along the weld path. Figure 1 presents the schematic drawing of the FSWed joint. In this method, the rotating tools can plastically deform (stir) and transport the surrounding material from the front to the back of the tools. So the workpieces can be stirred together to form a joint with good mechanical properties and better joint efficiency than the conventional welded joints [9]. The simultaneous rotation and traverse motion of the tool create asymmetrical temperature distribution and material flow between the two sides of the weld, which leads to different microstructures and mechanical properties between the advancing side (AS) and the retreating side (RS) of the weld [10]. The FSW process was considered

✉ M. Farahani
mrfarahani@ut.ac.ir

[1] School of Mechanical Engineering, College of Engineering, University of Tehran, Tehran, Iran

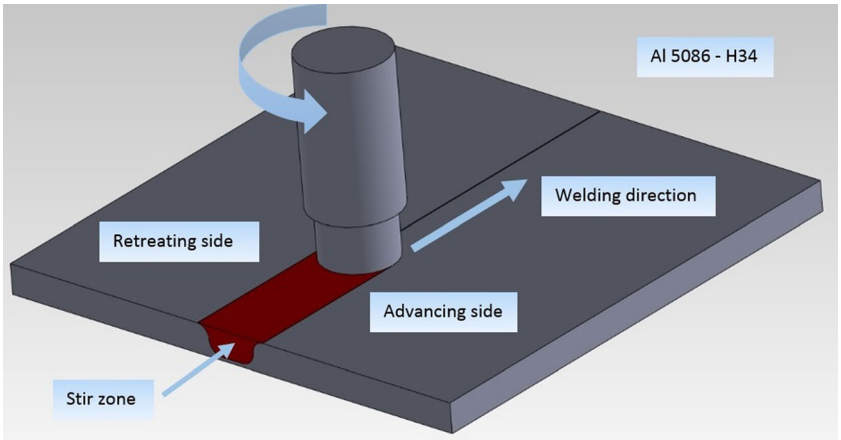

Fig. 1 The schematic drawing of the FSWed joint

to be the most significant development in metal joining in the past decades and due to energy efficiency, environment friendliness, and versatility, it is called a "green" technique. This method can be employed for joining the high-strength aluminum alloys and other metallic alloys, which cannot be easily welded through traditional fusion welding methods [11], but a few successful applications of FSW have been reported [12]. There is no liquid state for the weld pool during the FSW; as a result, the defect types within the weld, such as "tunnel defect," "lazy S," and "kissing-bond," can be seen in this type of welding. The tunnel defect is a long cavity in the weld along the welding direction as well; the lazy S is the oxide particle at the joint line remnant and the kissing bond is macroscopically a sound bonding, while it is an imperfect or weak bonding microscopically [13].

Friction stir welding has been recently applied for joining the Cu alloys [14–16], Al alloys [17–19], and Ti alloys [20, 21]. The obtained results presented an acceptable weld quality with applicable mechanical properties. Parameters including material and geometry of the tool, tilt angle, rotational speed, traverse speed, and vertical force of the tool significantly affects the friction stir welding process. These parameters affect the material transportation pattern and the welding temperature distribution during the welding process which consequently change the mechanical and metallurgical properties of these joints. In the present study, a combination of five rotational and three traverse speeds was used in friction stir welding of Al 5086-H34 alloy. The effects of tool rotational and traverse speeds on the microstructural and mechanical properties of the weld were studied, and the optimum process parameters were identified.

2 Materials and methods

In the present work, a 6-mm-thick aluminum plate of Al 5086-H34 with chemical composition as listed in Table 1 was utilized. Specimens with 100×50 mm dimensions were prepared for FSW.

Lots of studies were carried out to examine the influence of tool pin profile on the mechanical and microstructural properties of friction stir welded joint. Numerous application of the square pin profiled tool was observed in the contemporary literature [22–25]. Malik et.al. investigated the effects of six different tool pin profiles in friction stir welding. They observed that the square pin profiled tool consumes less power among other profiles employed in their study without affecting the temperature generation [23]. Venkata et al. examined the influence of tool pin profile on the microstructure and corrosion behavior of friction stir welded joint of AA2219 Al-Cu alloy. Their experiments were conducted with different tool pin profiles, namely conical, triangular, square, pentagon, and hexagon cross-sections. Appropriate properties were reported for the specimens prepared by the square pin profiled tool [24]. Amirafshar et al. studied the effect of tool pin design on the microstructural evolutions and tribological characteristics of friction stir processing. They observed that the tool pin designs of cylindrical, conical, and triangular, as well as square, are all successfully applicable for ST14 steel to produce defect-free processed material. According to their findings, the average grain size obtained with square profile was the minimum as compared to the obtained with conical, cylindrical, and triangular pins. The maximum hardness for stirred zone was also observed for specimens prepared by the square profiled tool [26]. Arora et al. reported that tools with flat faces such as square and triangular pin profiled tools created more heat during welding, so they were more susceptible to wear [27]. However, they observed that utilizing square pin profiled tool improved the mechanical and microstructural properties of the weldment due to the more imposed plastic deformation content and subsequent formation of grain boundaries rather than other pins. Bahrami et al. investigated the mechanical properties of the FSW joints using three different tools. They observed that using the square pin enhanced the tensile strength and elongation of the joints [28]. Elangovan et al.

Table 1 Chemical composition of Al 5086-H34 alloy (in wt.%)

Al	Si	Fe	Cu	Mn	Mg	Cr	Ni	Zn	Zr	Ti	Be	Bi	Ca	Li	Na	Pb	Sn	V
Base	0.142	0.362	0.0257	0.47	4.25	0.138	0.0062	0.0246	0.00079	0.0132	0.0024	0.0027	0.0022	<0.00005	0.0012	0.0031	0.0043	0.0078

investigated the mechanical properties of AA 6061 FSWed joints, utilizing five different tool profiles (square, triangular, threaded cylindrical, tapered cylindrical, and simple cylindrical). Results indicated that utilizing the tools with square pin led to superb microstructural and mechanical properties such as microhardness, ultimate tensile strength, and elongation [29]. The similar results were observed by Palanivel et al. [30].

Due to extensive application and great advantages of the square pin profiled tool, this configuration was employed in order to achieve the superb weld mechanical and microstructural properties. A tool from heat-treated H-13 hot work tool steel with the shoulder diameter of 16 mm, the pin diameter of 6 mm and, the pin height of 5.7 mm was employed. Figure 2 illustrates the geometry of the tool employed in this study.

In order to eliminate the tool wear, its hardness was increased to 52 HRC by heat treating. So no effective tool wear was observed even after several meters of 5086-H34 Aluminum welding.

In order to study the effects of process parameters on the microstructure and mechanical properties of 5086-H34 aluminum welded joints, full factorial experiments, including all combinations of five rotational speeds (RS) of 500, 800, 1000, 1250, and 1600 rpm and three traveling speeds (TS) of 41.5, 80, and 125 mm/min, were conducted as listed in Table 2.

In order to eliminate any marks left by the shoulder on the specimens, the top surfaces of the welded joints were machined. According to ASTM-E8, the sub-sized tensile specimens were cut from the welded samples perpendicular to the welding direction using electrical discharge machining [31]. The tensile tests were carried out using a SANTAM-STM50-type testing machine with a crosshead speed of 1 mm/min.

For metallographic examinations, the specimens were cross-sectioned perpendicular to the welding direction. Then, metallographic specimens were etched for 50 s using Poulton's reagent-solution. Grain size measurements were carried out according to ASTM E112-96. The fracture surface of the specimens was also examined using scanning electron microscopic (SEM). Besides, micro-hardness tests were carried out along a path perpendicular to the welding direction on the cross section of the specimens. A micro-hardness test machine with a Vickers indenter of 100 g load for 15 s was employed. The distance between the measurement points was selected to be 0.5 mm.

3 Results and discussion

3.1 Defects of friction stir welded joints

Insufficient heat generation and inadequate metal transportation increase the probability of defect formation [32]; therefore, it is necessary to select the tool rotational and traverse

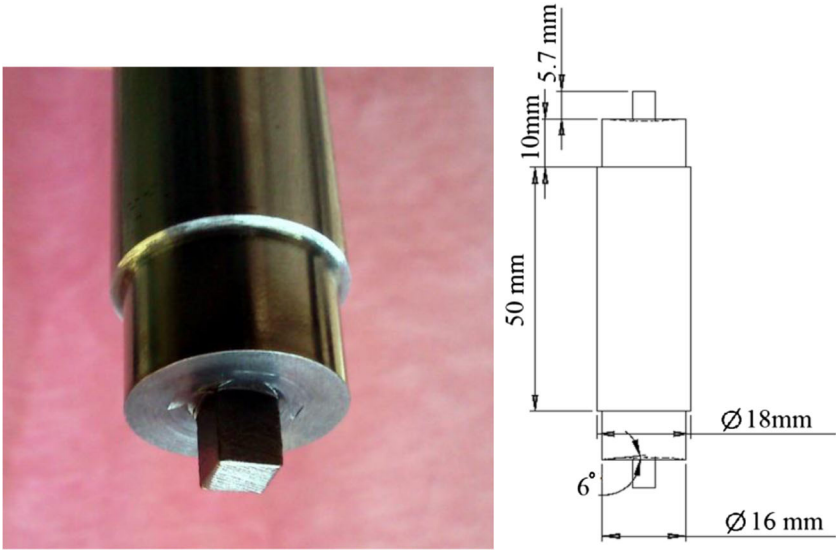

Fig. 2 The tool used in friction stir welding process

speeds carefully. Defects can seriously influence the mechanical properties of the weldment. The tensile strength and elongation of the weld were decreased significantly in the presence of weld defects as described by Chen et al.[33]. Figure 3 shows the macrostructure of the defective joints which are obtained with rotational speeds of 500, 800, and 1600 rpm.

Tunnel defects were observed at low rotational speeds (500 and 800 rpm) and very high rotational speed (1600 rpm). But there was not any defect in the cross section of the specimens prepared by rotational speeds of 1000 and 1250 rpm. Appropriate tool rotational and traverse speed provided a suitable welding heat input, which created a good condition for material stirring without any turbulences.

Basically, nugget shapes can be classified into two types, basin-shaped nugget that widens near the upper surface and elliptical nugget [12]. The shape of the nugget varies by the tool geometry and thermal conductivity of the base metal. As the tool geometry and the base metal were the same for all specimens, so uniform basin-shaped nugget for all samples were observed. The nuggets of the weld joints were widen near the upper surface except for the specimens prepared by rotational speed of 1600 rpm.

Table 2 Process parameters of the prepared FSWed joints

Rotational speed [rpm]	Traverse speed [mm/min]
500	41.5
500	80
500	125
800	41.5
800	80
800	125
1000	41.5
1000	80
1000	125
1250	41.5
1250	80
1250	125
1600	41.5
1600	80
1600	125

Figure 3 presents tunnel (worm hole) defects which were volumetric defects in continuous or non-continuous form. These defects were disrupted the weld in its severe forms and deteriorates the mechanical behavior of the joints. These defects acts as stress concentration centers in the weld section and decreased the strength of the welded joint significantly.

Formation of the tunnel defects at low rotational speeds of 500 and 800 rpm attributed to inadequate heat input and insufficient metal transportation. Besides, formation of defects at rotational speed of 1600 rpm can be explained by a further increase in the turbulence of the plasticized metal during welding at high rotational speeds. Rajakumar et al. also reported the formation of similar defects as a result of high tool rotation speeds [34]. Tunnel defects were observed on the lower side of the nuggets. Defect locations were depended on the material properties and the FSW parameters. In the examined specimens, the defects were normally observed on the advancing side of the weldment.

3.2 Microstructural examination

Figure 4 illustrates the microstructure of the base plate in its initial form. The images present the highly stretched grains of the rolled plate with an average length of 98 μm. The black and white regions shown in Fig. 4b indicates Al_xMg_y and Al_xMn_y compounds, respectively [35].

Figure 5 shows the distinct zones in the friction stir welded joint of Al 5086-H34: the stir zone (SZ), the thermo-

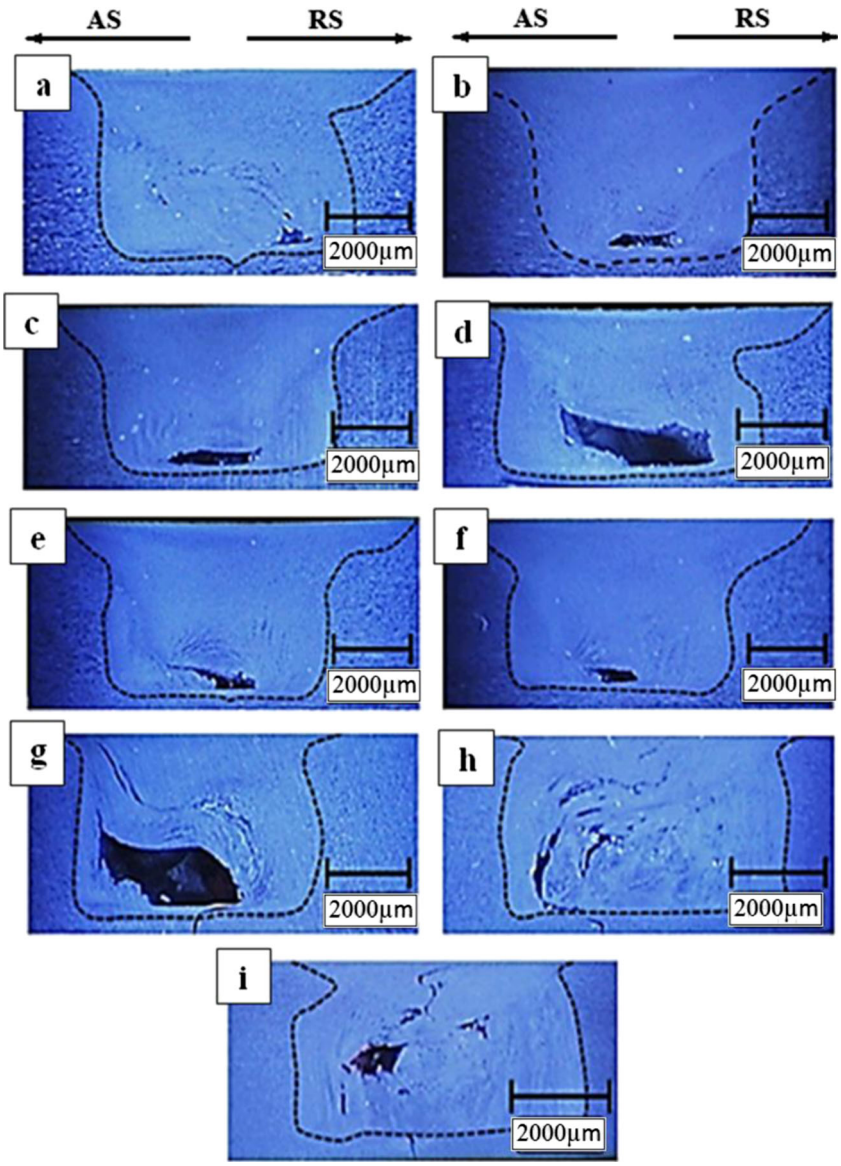

Fig. 3 Cross-section view of the defective welds with rotational and traverse speeds of **a** 500 rpm, 41.5 mm/min; **b** 500 rpm, 80 mm/min; **c** 500 rpm, 125 mm/min; **d** 800 rpm, 41.5 mm/min; **e** 800 rpm, 80 mm/min; **f** 800 rpm, 125 mm/min; **g** 1600 rpm, 41.5 mm/min; **h** 1600 rpm, 80 mm/min; **i** 1600 rpm, 125 mm/min

mechanically affected zone (TMAZ,) and the base metal (BM). The SZ had fine grains with recrystallized equiaxed grain structure as observed in ref. [36]. The frictional heating and extensive plastic deformation generate fine grains in the nugget zone [37]. Nelley et al. attributed the miniaturization of the aluminum grains to high stacking fault energy and dynamic mechanical recrystallization during welding [38]. The bending of the grains in the TMAZ can be explained by the stirring action of the FSW tool which drawn the flat grains of the parent metal into the weld nugget zone [22]. The most decrease in grain size was observed at the boundaries between the TMAZ and HAZ [39].

In order to study the effects of welding rotational and traverse speed on the microstructure of the welded joints, the microstructures of the SZ for sound welded joints are presented in Fig. 10. Intensive temperature rise and severe plastic deformation during FSW lead to the formation of fine equiaxed microstructure in the SZ. Dynamic recovery (DRV), geometric dynamic recrystallization (GDRX), and discontinuous dynamic recrystallization (DDRX) are the mechanisms which refine the grains during the FSW. DDRX normally begins at the old grain boundaries. New grains are then nucleated at the boundaries of the growing grains, and in this way, a thickening band of recrystallized grains is shaped. This phenomena is named the discontinuous dynamic recrystallization [22]. Severe plastic deformation during the FSW breaks the grains and generates low angle misorientated grain boundaries and suitable sites for nucleating recrystallization. Dynamic recrystallization transforms the low-angle grain boundaries to high-angle grain boundaries and produced fine equiaxed grains [40].

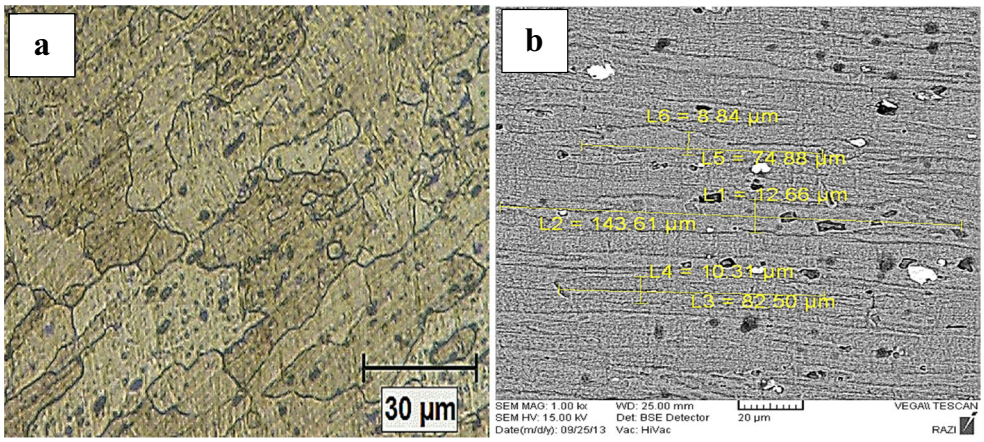

Fig. 4 Microstructure images of the base plate using **a** optical microscopy (OM) and **b** SEM

Increase of tool traverse speed led to more plastic deformation in the weld zone. Comparison between Fig. 6a and c revealed that the grain size of the SZ reduced by increasing the traverse speed which can be explained by the more dynamic recrystallization and also the less annealing effect of the welding heat input at higher traverse speed. The similar results were obtained by comparing the Fig. 6d with Fig. 6f.

Grain size measurements were carried out according to ASTM E112-96. The measured grain sizes for different specimens are listed in Table 3. Figure 7 presents the effects of rotational and traverse speeds on the average grain size of the welded specimens. Two key factors affect the grain size in the SZ: the first one is the dynamic recrystallization and increases in the dislocation density, which consequently prevents the grain boundary slipping and reduces the grain size, and the second one is the annealing effect of the welding heat input, which increases the grain size [41].

By increasing the traverse speed, the material underwent severe mechanical stresses and experienced an extensive dynamic recrystallization, which increased the number of nucleation sites and reduced the grain size. On the other side, decrease in the welding heat input at high traverse speeds mitigated the effects of annealing. The heat input reduction occurred as the result of reduction in the stirring process. Due to these two mechanisms, the grain size decreased significantly with an increase in the traverse speed, which presented in Fig. 7.

It is also observed that an increase in the rotational speed amplified the stirring effect and resulted in more material deformation and stirring which decreased the grain size significantly.

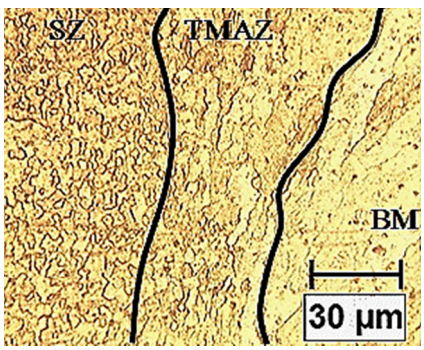

Fig. 5 SZ and TMAZ in the friction stir welded joint

3.3 Mechanical properties

3.3.1 Hardness results

In the following, the effects of rotational and traverse speeds on the microhardness of the prepared samples were studied. The microhardness measurement for 30 points in the aluminum 5086-H34 was 89±2. 2 HV. Figure 8 represenst the microhardness variations of the welded specimens at rotational speeds of 1000 and 1250 rpm, respectively. In all cases, the microhardness of the SZ was greater than the base metal hardness. Besides, it was observed that the microhardness values of the TMAZ were a little lower than the microhardness of the base metal which might be due to dissolution and growth of the precipitates during the welding. Similar results were observed by Yadav et al. [42]. No meaningful changes in TMAZ hardness were observed by changing the welding process parameters.

The annealing effect and stirring action are the two main factors which affect the microhardness of the joints. Stirring action of the pin was raised by increasing the tool rotational speed. Higher stirring action of the pin led to more dynamic recrystallization which reduced the grain size, increased the dislocations, and finally improved the microhardness of the SZ. The increment of the microhardness of the SZ due to grain miniaturization can be described by the Hall-Petch relationship [43]. On the other hand, the annealing effect of welding

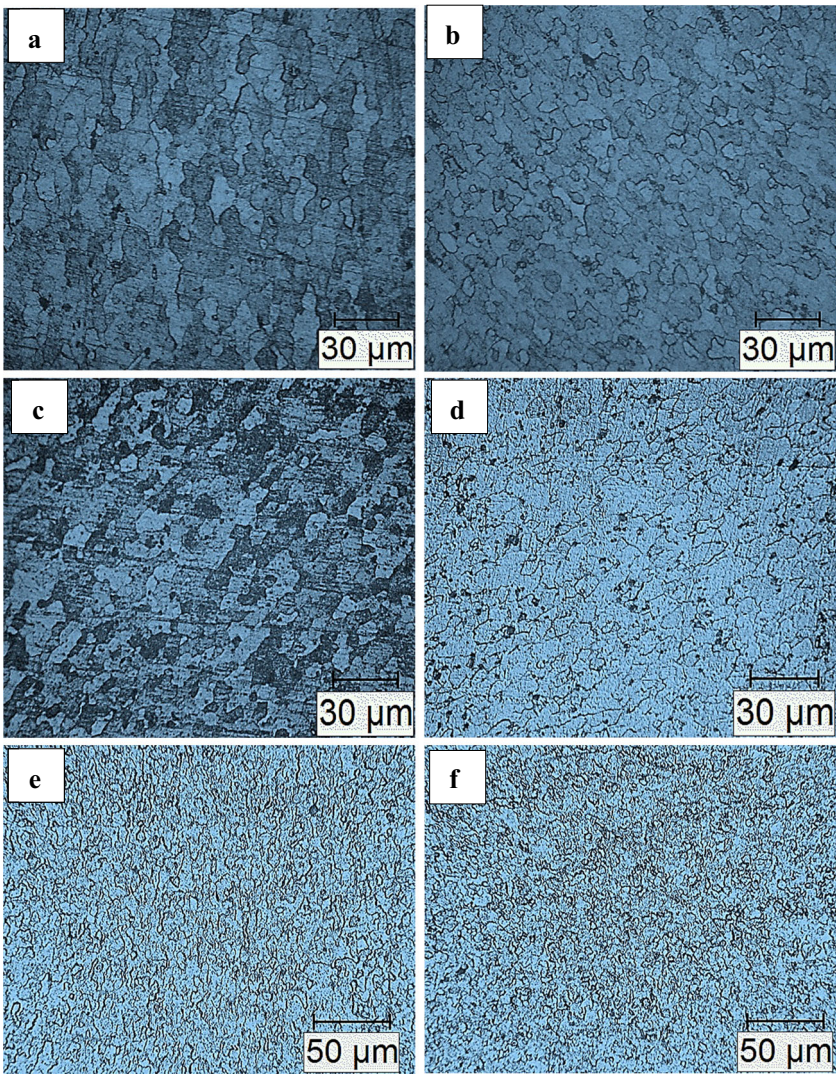

Fig. 6 The microstructure of the SZ for specimens with rotational and traverse speeds of **a** 1000 rpm and 41.5 mm/min, **b** 1000 rpm and 80 mm/min, **c** 1000 rpm and 125 mm/min, **d** 1250 rpm and 41.5 mm/min, **e** 1250 rpm and 80 mm/min, and **f** 1250 rpm and 125 mm/min

heat input declined the microhardness of the joints. In friction stir welding of Al 5086-H34, the effect of stirring action on high tool rotational speed was dominant, so the microhardness of the SZ was increased at higher rotational speed. A further increase in the microhardness of the SZ was observed at higher welding traverse speed, which was due to the lower welding heat input and consequently the lower annealing effect. Meanwhile, more material deformation at higher traverse speeds increased the dislocation density and consequently increased the hardness of the SZ.

Table 3 The grain size of the FSW joints with different rotational and traverse speeds

Rotational speed	1000 rpm			1250 rpm		
Specimen's number	1	2	3	4	5	6
Traveling speed (mm/min)	41.5	80	125	41.5	80	125
Grain size (μm)	14.2	12.7	11.8	10.9	9.8	7.6

It is evident in Fig. 8 that the microhardness values in the advancing side were higher than the retreating side. This is due to the asymmetric and non-uniformed material transportation through the welding. The higher hardness with more

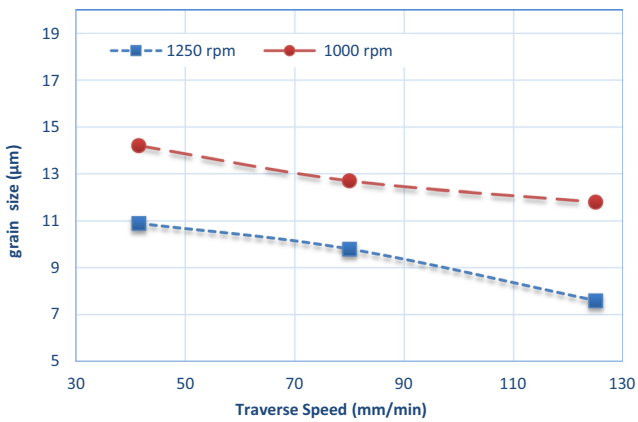

Fig. 7 Mean grain size variations for different rotational and traverse speeds

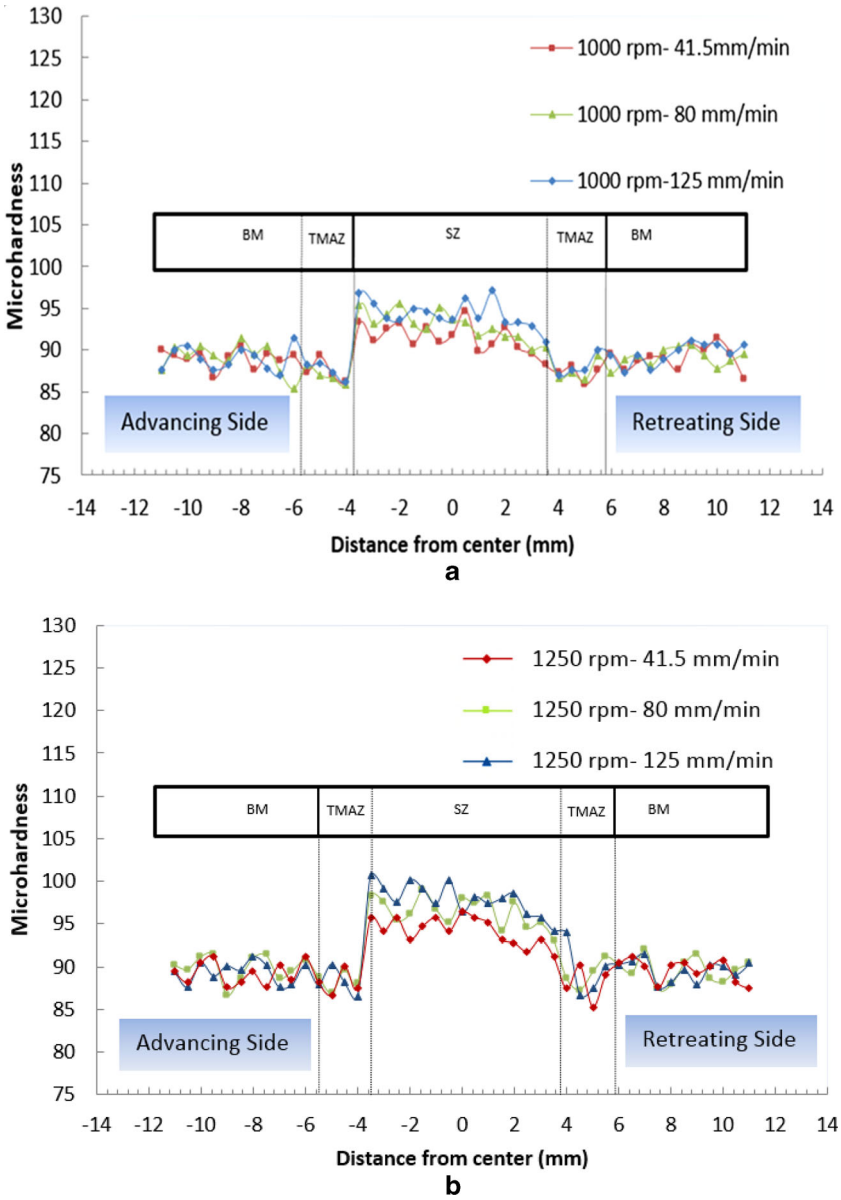

Fig. 8 Microhardness of FS welded specimens in different traverse speeds and rotational speed of **a** 1000 and **b** 1250 rpm

high-angle grain boundaries in the advancing side proved that the dislocation hindrance mechanism (at grain boundaries) had a significant role in the enhancing the microhardness of the weldment [44]. The lower hardness of the TMAZ than the

Table 4 Mechanical properties of the FSW joints with different rotational and traverse speeds

Rotational speed	1000 rpm			1250 rpm		
Specimen's number	1	2	3	4	5	6
Traveling speed (mm/min)	41.5	80	125	41.5	80	125
Percentage of elongation	16.5	13	12	18	23.5	24
UTS (MPa)	167	182	229	233	264.5	252

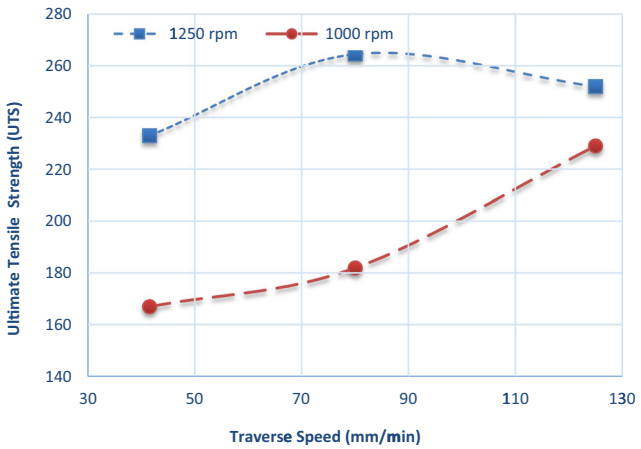

Fig. 9 Ultimate tensile strength for different rotational and traverse speeds

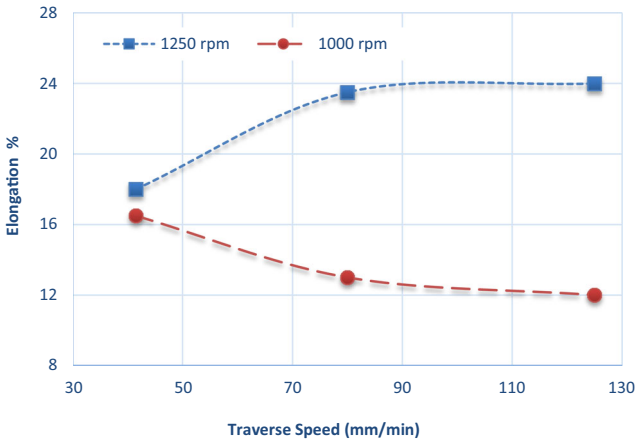

Fig. 10 Elongation for welded joints with different rotational and traverse speeds

base metal in welded specimens might be due to dissolution and deposit growth in this zone.

3.3.2 Tensile results

Tensile tests were performed at room temperature in order to study the effects of rotational and traverse speeds on the ultimate tensile strength (UTS) and elongation of the welded specimens. The measured UTS band elongation for the base metal were 310 MPa and 15.5 %, respectively. Tensile properties including UTS and elongation of the studied samples are presented in Table 4.

The UTS of all the welded joints were smaller than the base metal ultimate strength. An increase in tool rotational speed increased the UTS of the welded joints significantly. It can be explained by the significant decrease in the grain size at high rotational speeds. Figure 9 shows the variation of the UTS of the welded joint at different rotational and traverse speeds.

By increasing the traverse speed at the constant rotational speed of 1000 rpm, the UTS of the welded joints was increased. As the grain size of the specimens decreased, the UTS of the welded joins were increased. But at the rotational speed of 1250 rpm, the maximum UTS was obtained for the specimens prepared by the traverse speed of 80 mm/min, while a further increase in the welding speed results in a decrease of the UTS of the welded joints. This was due to the insufficient frictional heat generated. In general, FSW at higher traverse speeds resulted in a short exposure time in the weld area with insufficient heat and a poor plastic flow of the metal which caused some void-like defects in the joints. Investigations of Palanivel et al. were in good agreement with the aforementioned results [23]. It can be concluded that in

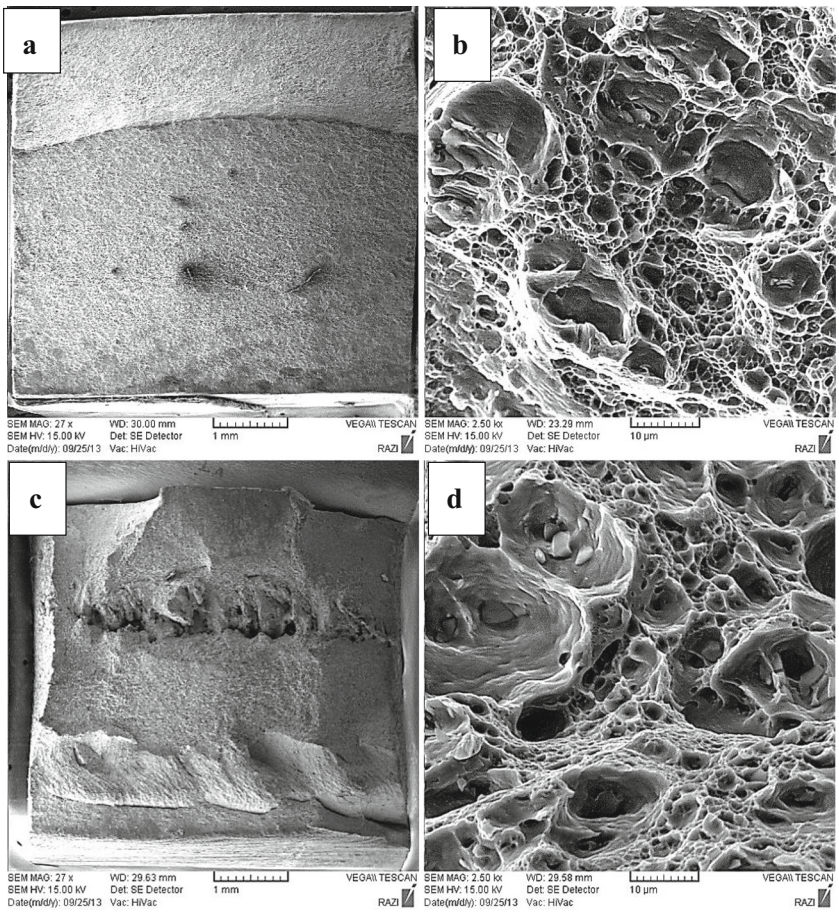

Fig. 11 Low and high magnification fractographs of **a**, **b** base metal and **c**, **d** welded joint with rotational speed of 1250 rpm and traverse speed of 80 mm/min

order to achieve the maximum strength for each rotational speed, an optimal traverse speed should be employed. The optimum traverse speed for rotational speed of 1000 rpm is probably higher than 125 mm/min.

The elongation in some of the specimens increased significantly in comparison to the base metal. It can be described by the release of compressive residual stresses generated during the rolling of the base metal. The similar results were reported by Barmouz et al. [45]. The elongation variations of the welded specimens for different rotational and traverse speeds are presented in Fig. 10.

Grain size and dispersion of precipitated second phase particles are the two factors which affect the elongation of the welded specimens. At rotational speeds of 1250 rpm, the grain size of the SZ decreased by increasing the tool rotational speed and consequently the ductility of the specimens increased. But at a rotational speed of 1000 rpm, poor plastic flow of the material by increasing the traverse speed led to nonuniform dispersion of precipitated second phase particles in the Al matrix which reduced the elongation.

Figure 11 illustrates the fracture surfaces of the base metal and the specimen with the largest UTS (rotational speed of 1250 rpm and traverse speed of 80 mm/min).

As shown in Fig. 4b, d, the dimple pattern of the welded specimens was smaller than the base metal, which resulted in ductile fracture. The UTS and elongation in this specimen were about 78 and 111 % of the base metal, respectively, which confirmed this observation.

4 Conclusion

In this study, FSW was applied for butt joining of the aluminum 5086-H34 alloy plates at different rotational and traverse speeds. The effects of rotational and traverse speeds were investigated on the mechanical and microstructural properties of the welded joints. The results can be summarized as follows:

- At very low rotational speeds, tunneling and worm hole defects were generated as a result of insufficient heat generation and insufficient metal transportation.
- At very high rotational speeds, the large turbulence in the plasticized metal led to tunneling and worm hole defects.
- Increase of the tool rotational and traverse speed led to grain refinement which induced by the intensive dynamic recrystallization and the increase of dislocation density.
- An increase in the tool rotational speed increased the UTS of the welded joints significantly. In order to achieve the maximum joint strength for each rotational speed, an optimal traverse speed should be employed.
- Using higher traverse speed increased the microhardness of the specimens which can be explained by a decrease in the welding heat input and further material deformation at higher tool traverse speed.
- The microhardness of the thermo-mechanically affected zone was lower than the base metal which can be attributed to dissolution and growth of the precipitates during the welding.

Acknowledgments The authors are grateful for the support of the Iran National Science Foundation (INSF) in Project No. 9100812.

References

1. Aydın H, Bayram A, Uğuz A, Akay KS (2009) Tensile properties of friction stir welded joints of 2024 aluminum alloys in different heat-treated-state. Mater Des 30:2211–2221
2. Xu W, Liu J, Luan G, Dong C (2009) Temperature evolution, microstructure and mechanical properties of friction stir welded thick 2219-O aluminum alloy joints. Mater Des 30:1886–1893
3. Farahani M, Sattari-Far I, Akbari D, Alderliesten R (2012) Numerical and experimental investigations of effects of residual stresses on crack behavior in Aluminum 6082-T6. Proc Inst Mech Eng C J Mech Eng Sci 226:2178–2191
4. Farahani M, Sattari-Far I (2011) Effects of residual stresses on crack-tip constraints. Scientia Iranica B 18(6):1267–1276
5. Farahani M, Sattari-Far I, Akbari D, Alderliesten R (2013) Effect of residual stresses on crack behaviour in single edge bending specimens. Fatigue Fracture Eng Mat Struct 36:115–126
6. Zargar S, Farahani M, Besharati M (2015) Numerical and experimental investigation on the effects of submerged arc welding sequence on the residual distortion of the fillet-welded plates. Proceedings of the Institution of Mechanical Engineers, Part B: J Eng Manufac
7. Kumbhar NT, Sahoo SK, Samajdar I, Dey GK, Bhanumurthy K (2011) Microstructure and microtextural studies of friction stir welded aluminium alloy 5052. Mater Des 32:1657–1666
8. Bagheri Hariri M, Gholami Shiri S, Yaghoubinezhad Y, Mohammadi Rahvard M (2013) The optimum combination of tool rotation rate and traveling speed for obtaining the preferable corrosion behavior and mechanical properties of friction stir welded AA5052 aluminum alloy. Mater Des 50:620–634
9. Yufeng S, Nan X, Yoshiaki M, Hidetoshi F (2012) Microstructure and mechanical properties of friction stir welded pure Cu plates. Trans JWRI 41:53–58
10. Shi L, Wu C, Liu H (2015) The effect of the welding parameters and tool size on the thermal process and tool torque in reverse dual-rotation friction stir welding. Int J Mach Tools Manuf 91:1–11
11. Wu H, Chen Y-C, Strong D, Prangnell P (2015) Stationary shoulder FSW for joining high strength aluminum alloys. J Mater Process Technol 221:187–196
12. Mishra R, Ma Z (2005) Friction stir welding and processing. Mater Sci Eng 50:1–78
13. Li W, Li J, Zhang Z, Gao D, Chao Y (2013) Metal flow during friction stir welding of 7075-T651 aluminum alloy. Exp Mech 53: 1573–1582
14. Shen Z, Chen Y, Haghshenas M, Nguyen T, Galloway J, Gerlich AP (2015) Interfacial microstructure and properties of copper clad steel produced using friction stir welding versus gas metal arc welding. Mater Charact 104:1–9
15. Yufeng S, Nan X, Yoshiaki M, Hidetoshi F (2012) Microstructure and mechanical properties of friction stir welded pure Cu plates. Trans JWRI 41:53–58

16. Ouyang J, Yarrapareddy E, Kovacevic R (2006) Microstructural evolution in the friction stir welded 6061 aluminum alloy (T6-temper condition) to copper. J Mater Process Technol 172:110–122
17. Jamshidi Aval H, Serajzadeh S, Kokabi A (2012) Experimental and theoretical evaluations of thermal histories and residual stresses in dissimilar friction stir welding of AA5086-AA6061. Int J Adv Manuf Technol 61:149–160
18. Cavaliere P (2013) Friction stir welding of Al alloys: analysis of processing parameters affecting mechanical behavior. Proc CIRP 11:139–144
19. Dawood HI, Mohammed KS, Azmi R, UdayDawood MB (2015) The influence of the surface roughness on the microstructures and mechanical properties of 6061 aluminium alloy using friction stir welding. Surf Coat Technol 270:272–283
20. Mironov S, Sato Y, Kokawa H (2009) Development of grain structure during friction stir welding of pure titanium. Acta Mater 57: 4519–4528
21. Fratini L, Micari F, Buffa G, Ruisi VF (2010) A new fixture for FSW processes of titanium alloys. CIRP Ann Manuf Technol 59(1): 271–274
22. Besharati Givi M, Asadi P (2014) Advances in friction-stir welding and processing, 1st Edition. Woodhead Publishing
23. Malik V, Sanjeev NK, Hebbar HS, Kailas SV (2014) Investigations on the effect of various tool pin profiles in friction stir welding using finite element simulations. Proc Eng 97:1060–1068
24. Venkata Rao C, Madhusudhan Reddy G, Srinivasa Rao K (2015) Influence of tool pin profile on microstructure and corrosion behaviour of AA2219 Al–Cu alloy friction stir weld nuggets. Defence Technology, In Press
25. Suri A (2014) An improved FSW tool for joining commercial aluminum plates. Proc Mat Sci 6:1857–1864
26. Amirafshar A, Pouraliakbar H (2015) Effect of tool pin design on the microstructural evolutions and tribological characteristics of friction stir processed structural steel. Measurement 68:111–116
27. Arora A, Mehta M, De A, DebRoy T (2012) Load bearing capacity of tool pin during friction stir welding. Int J Adv Manuf Technol 61: 911–920
28. Bahrami M, Farahmand Nikoo M, Besharati Givi M (2015) Microstructural and mechanical behaviors of nano-SiC-reinforced AA7075-O FSW joints prepared through two passes. Mater Sci Eng A 626:220–228
29. Elangovan K, Balasubramanian V (2008) Influences of tool pin profile and tool shoulder diameter on the formation of friction stir processing zone in AA6061 aluminium alloy. Mater Des 29(2): 362–373
30. Palanivel R, Koshy Mathews P (2011) The tensile behaviour of friction stir welded dissimilar aluminium alloys. Mat Technol 45: 623–626
31. Bahrami M, Dehghani K, Besharati Givi M (2014) A novel approach to develop aluminum matrix nano-composite employing friction stir welding technique. Mater Des 53:217–225
32. Sun Y, Fujii H (2010) Investigation of the welding parameter dependent microstructure and mechanical properties of friction stir welded pure copper. Mater Sci Eng A 527:6879–6886
33. Chen H, Yan K, Lin T, Chen S, Jiang C, Zhao Y (2006) The investigation of typical welding defects for 5456 aluminum alloy friction stir welds. Mater Sci Eng A 433:64–69
34. Rajakumar S, Balasubramanian V (2012) Establishing relationships between mechanical properties of aluminium alloys and optimised friction stir welding process parameters. Mater Des 40:17–35
35. ASM Handbook, Alloy Phase Diagrams (1992) The Materials Information Company
36. Lee W-B, Jung S-B (2004) The joint properties of copper by friction stir welding. Mater Lett 58(6):1041–1046
37. Ma Z, Mishra R, Mahoney M (2002) Superplastic deformation behaviour of friction stir processed 7075Al alloy. Acta Mater 50: 4419–4430
38. McNelley TR, Swaminathan S, Su JQ (2008) Recrystallization mechanisms during friction stir welding/processing of aluminum alloys. Scr Mater 58:349–354
39. Kasman Ş, Yenier Z (2013) Analyzing dissimilar friction stir welding of AA5754/AA7075. Int J Adv Manuf Technol 70:145–156
40. Dolatkhah A, Golbabaei P, Besharati Givi MK, Molaiekiya F (2012) Investigating effects of process parameters on microstructural and mechanical properties of Al5052/SiC metal matrix composite fabricated via friction stir processing. Mater Des 37:458–464
41. Barmouz M, Besharati Givi MK, Seyfi J (2011) On the role of processing parameters in producing Cu/SiC metal matrix composites via friction stir processing: Investigating microstructure, microhardness, wear and tensile behavior. Mater Charact 62:108–117
42. Yadav D, Bauri R (2012) Effect of friction stir processing on microstructure and mechanical properties of aluminium. Mater Sci Eng A 539:85–92
43. Ma ZY (2008) Friction stir processing technology: a review. Metall Mater Trans A 39(3):642–658
44. Yadav D, Bauri R (2012) Effect of friction stir processing on microstructure and mechanical properties of aluminium. Mater Sci Eng A 539:85–92
45. Barmouz M, Asadi P, Besharati Givi MK, Taherishargh M (2011) Investigation of mechanical properties of Cu/SiC composite fabricated by FSP: effect of SiC particles' size and volume fraction. Mater Sci Eng A 528:1740–1749